Chapter 2
Acute Neural Stimulation

2.1 Introduction

In the previous chapter, I discussed the advantages of using nanotechnologies to probe the mechano-biology of the brain. In this chapter, I describe the development of a magnetic microfabricated substrate and magnetic nanoparticle technology to induce calcium influx in neural networks by enhancing the opening probability of mechano-sensitive N-type Ca^{2+} channels.

As a second messenger in a plethora of signaling pathways, spatial and temporal variation in intracellular calcium (Ca^{2+}) influxes has been shown to induce gene transcription, and influence mRNA translation and even posttranslational protein modification [1]. However, in order to act as a specific second messenger, cytoplasmic Ca^{2+} concentration is maintained at a much lower concentration (100–300 nM) compared to extracellular spaces (1–3 mM) and endoplasmic reticulum (10–100 μM) [2]. To spatially and temporally activate signaling in cells, there is thus significant interest to manipulate Ca^{2+} levels, especially in neurons where Ca^{2+} dynamics within dendritic spines are associated with synaptic plasticity in neural networks [3], learning, and behaviors [4].

Intracellular Ca^{2+} concentrations have been controlled with electricity, chemical stimulation, ultrasound, heat, and even light [5]. The earliest attempts to control Ca^{2+} levels in neurons employed electrodes and chemical delivery systems that allowed temporal control but were unable to provide localized stimulation to densely packed neural tissues [6]. Ultrasound stimulation of ion channels can remote trigger calcium influxes although it is still largely limited by its nonspecificity (space and time) on the neural networks and its potential side effects of heating [7, 8]. The progress in optogenetics has demonstrated the utility of light to activate photosensitive ion channels in neurons specifically [6, 9, 10]. Nonetheless, these techniques necessitate complex modification of exogenous genes to express photosensitive ion channels or delivery of photosensitive ligand to specific receptors on neurons which are either irreversible or require a long time for effects to diminish. Optical

A.K.P. Tay, *Acute and Chronic Neural Stimulation via Mechano-Sensitive Ion Channels*, Springer Theses, https://doi.org/10.1007/978-3-319-69059-9_2

approaches in general are still limited by the poor penetration of visible light into deep tissues and its resolution hinges heavily on the precision of the optical fibers used for light delivery [11].

Magnetic fields are ideal for noninvasive manipulations as they can achieve deep tissue penetration and localization by tuning force-inducing field gradients. To overcome the weak interaction between magnetic fields and biological molecules, magnetic fields should be translated into mechanical forces or torques [12, 13] such as during magnetic resonance imaging (MRI) in the latter case. One way of achieving this is through ferromagnetic nanoparticles (MNPs) that bind to cell membrane receptors or are internalized into the neurons followed by subsequent exposure of the neurons to magnetic field gradients.

Huang et al. [14] and recently Chen et al. [15] made use of low-radiofrequency alternating magnetic field-induced heating to stimulate the opening of temperature-sensitive ion channels (TRPV1) in rat neurons. Although high-amplitude Ca^{2+} influxes were observed in the latter case, Chen and coworkers did not comprehensively investigate the effects of sustained heating, heating due to internalized MNPs, and heat diffusion to non-targeted sites at noxiously high temperature of 43 °C. The use of this technique for therapeutic treatments of human neuro-diseases may also face several challenges: (1) nonspecific activation due to various endogenous chemical agonists such as lipoxygenase products [5] to mammalian TRPV1 receptor and (2) potential complications with viral delivery agents and gene therapies.

Very recently, Marino et al. also demonstrated the use of ultrasound to activate piezoelectric nanoparticles to induce Ca^{2+} influxes in individual neurons differentiated from human neuroblastoma-derived cells [8]. However, in their technology, there was no indication that the Ca^{2+} influxes were propagated in the neural network. As the neural network paradigm gains traction and importance for the investigation of brain-related activities [16], it is important to demonstrate the propagation of Ca^{2+} influxes in neural networks to better predict in vivo behavior. In addition, although there were some cases of high Ca^{2+} influxes, the heterogeneity in sizes of differentiated neurons complicates the fluorescence quantification [17]. Essentially, larger cell bodies are expected to have larger Ca^{2+} influxes and vice versa. Lastly, while ultrasound technology is improving, its poor penetration though the human skulls can limit downstream application of this technology [18].

In summary, an ideal method for remote stimulation of neural network should be noninvasive, safe under long duration exposure, spatially and temporally controllable, and with different degrees of activation.

Previous studies have shown that internalized MNPs can stop neurite outgrowth with forces in the low pico-Newton (pN) range [19]. Our group demonstrated that localized mechanical stimuli due to magnetic fields can alter intracellular distributions of the microtubule-associated protein tau [20]. Related work using magnetic force was also presented by Etoc and colleagues [21]. Additionally, MNPs have reportedly affected gene regulation and Ca^{2+} influx [22] and lowered threshold and duration of action potential [23]. These observations suggest that low pN range

mechanical forces induced by magnetic fields may be capable of influencing signal transduction in neurons. However, the technical difficulty of performing electrophysiological recordings with magnetic force stimulation has not allowed the mechanisms giving rise to Ca^{2+} influx to be investigated.

Here, we demonstrate that nano-magnetic force stimulation with MNPs could induce Ca^{2+} influx within in vitro-grown cortical neural networks and heighten the magnitude and frequency of intracellular Ca^{2+} waves. Stimulated cortical neural networks showed an average 20% increment in Ca^{2+} fluorescence signals, with the effects having a spatial resolution of 200 μm. Additionally, inhibition of Ca^{2+} influx in the presence of nano-magnetic forces by ω-conotoxin, an N-type Ca^{2+} channel inhibitor, implicated mechano-sensitive ion channels as responsible for Ca^{2+} influxes. Our findings support the hypothesis that magnetic forces can induce Ca^{2+} influxes that would likely mediate the growth of neurite [24] and intracellular distribution of proteins [20, 25] and suggest the use of wireless magnetic forces to remotely modulate neural network activity.

2.2 Results and Discussions

2.2.1 Experimental Setup

Primary dissociated cortical neurons were plated onto poly-L-lysine (PLL, 20–100 μm) stripes on a neuro-magnetic chip that guided network growth during culture (Fig. 2.1a, b). Two-week-old cortical neural networks were then incubated with MNPs and stimulated with nano-magnetic forces within an engineered magnetic field of 150 mT maximum strength (~110 mT) at the chip surface about 1 μm above the permalloy elements as characterized previously in [20]. The dimensions of the magnetic elements in combination with the observed cluster size of MNPs exert forces in the pico-Newton range (Fig. 2.1c). Fluorophores were used to monitor Ca^{2+} fluctuations in the cortical neural network followed by data analyses (Fig. 2.1d).

2.2.2 Characterization of Starch- and Chitosan-Coated MNPs

Starch-coated and chitosan-coated MNPs were used for this application due to their commercial availability and previous uses in neural related applications with low cytotoxicity (Appendix A Table A.1). The hydrodynamic sizes of the MNPs measured in conditioned media through dynamic light scattering were 209 ± 9 nm (starch) and 588 ± 31 nm (chitosan). The polydispersity index was similar for both MNPs in the range of 0.200–0.210. The zeta potentials were −30.9 ± 2 mV

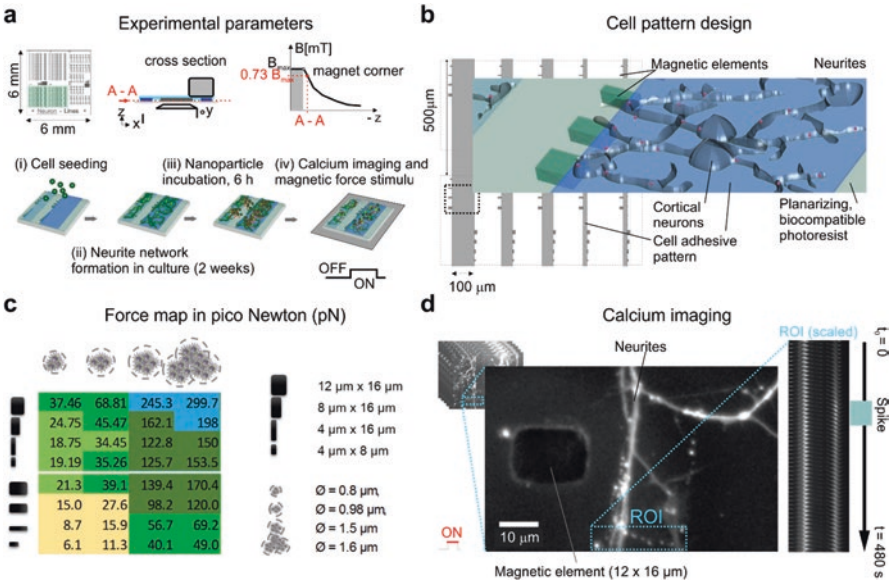

Fig. 2.1 Experimental workflow for nano-magnetic force-based triggering of calcium influx. (**a**) Schematic shows chip dimensions, experimental setup, and applied magnetic field approximation (B_{max} = 150 mT: ON, B: 0 mT: OFF). At 1 µm above the permalloy elements, the magnetic field strength is ~0.73*B_{max} = ~110 mT as determined by monitoring movements of magnetic microparticles in applied magnetic fields. The workflow is composed of the following: (i) Seeding of neuronal cell (830,000 cells/cm^2) on spatially controlled cell adhesive patterns (PLL/Pluronics) on the magnetic chip, (ii) formation of neurite networks over 2 weeks in culture, (iii) incubation with ferromagnetic nanoparticles (MNPs, 54,000 × 10^6/mL) for 6 h followed by subsequent washing, and (iv) loading with calcium dye (fluo-4) and stimulation with a permanent magnetic field (B_{max}: 150 mT). (**b**) Cell adhesive pattern design of 100, 50, and 20 µm width lines allows neurite network growth adjacent to magnetic elements on the magnetic chip over 2 weeks. Repetitive pattern design (here 500 µm spaced) supports parallelization of experiments. (**c**) Force map shows estimated peak magnetic forces at 1 µm distance above the magnetic elements in combination with four different fMNP cluster diameters [20]. (**d**) On chip image acquisition of calcium activity (fluo-4 with probenecid acid). Extracted fluorescent signal from local regions of interest (ROI) exhibits stimulated calcium spike activity with starch-coated MNPs

(starch) and −21.0 ± 7 mV (chitosan), highlighting high stability of the dispersion (Appendix A Table A.2). We characterized the properties of the MNPs in conditioned media as we believe that cells can actively secrete molecules into the media or deplete molecules from the media in response to added nanoparticles. This would thus modify the protein corona on the MNPs [26], thus impacting interaction with membrane proteins, endocytosis, and intracellular fate of the MNPs [27]. There is also now increasing evidence that protein coronas can predict the interactions between nanoparticles and cells more effectively than size and surface charge [26].

2.2.3 *Location and Uptake of MNPs*

To better evaluate the interactions between cortical neurons and MNPs, we determined the uptake of MNPs by the cortical neural network through flow cytometry. Following 24-h incubation, 34.8% of the cortical neurons had uptaken starch-coated MNPs while 68.4% had uptaken chitosan-coated MNPs (Fig. 2.2a). Although the former has a smaller hydrodynamic diameter, its zeta potential is more negative, possibly leading to increased repulsion with negatively charged cell membrane [28] and lower uptake.

However, we recognize that a major limitation in using flow cytometry is the inability to differentiate whether the nanoparticles are localized inside the cells, on the cell membrane or at other parts of the cell (such as soma and neurites) [27]. Therefore, we depleted the energy of the cortical neurons with sodium azide to

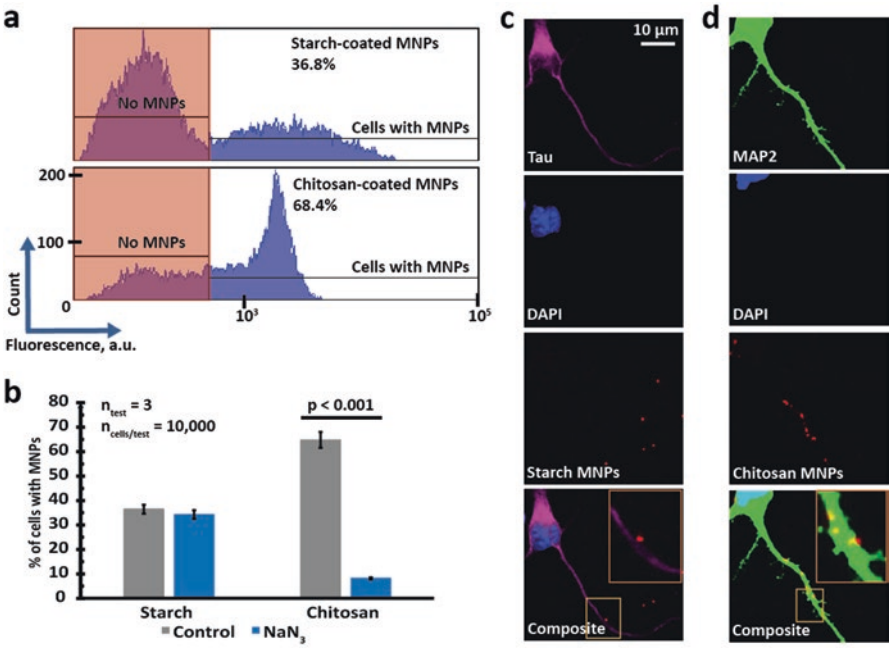

Fig. 2.2 Nanoparticles interacted differently with cortical neural network. (**a**) Flow cytometry analysis showed that cortical neural network uptakes less starch-coated MNPs than chitosan-coated MNPs. However, one limitation of flow cytometry is the inability to differentiate particles that are internalized or associated with the membranes. (**b**) Sodium azide (5 mg/mL) was added to inhibit endocytosis. Results from flow cytometry revealed that chitosan-coated MNPs were internalized into cortical neural network via endocytosis but starch-coated MNPs were most likely associated with the membrane. (**c**) Fluorescent images confirmed that starch-coated MNPs were mostly associated with the neurites while (**d**) chitosan-coated MNPs were internalized and localized with lysosomes

inhibit endocytosis, an energy-dependent process [29]. The addition of sodium azide reduced endocytosis of chitosan-coated MNPs by close to 90% but had no significant effects on starch-coated MNPs (Fig. 2.2b). This meant that most starch-coated MNPs were not internalized by the cortical neurons but were instead associated with the cell membranes. On the other hand, chitosan-coated MNPs were internalized into the cortical neurons.

Next, we performed confocal fluorescence imaging to identify whether there was a preferential localization of the MNPs on any particular structure of the cortical neural network. This was because we hypothesized that the nano-magnetic forces might activate mechano-sensitive Ca^{2+} ion channels which are found in higher density along the neurites [30]. We found that chitosan-coated MNPs tended to be internalized along the neurites (Fig. 2.2d). On the other hand, starch-coated MNPs preferred to localize at the membranes (Fig. 2.2c). While the reasons for these localization behaviors are still largely unclear, it has previously been reported that chitosan can bind to CD44 receptors of cancer stem cells [31] and a similar receptor-mediated mechanism may be responsible where the neurites may present membrane receptors that can bind to starch.

2.2.4 *Nano-Magnetic Forces Induce Ca^{2+} Influxes*

We first demonstrated that nano-magnetic forces could induce Ca^{2+} influx in cortical neural networks with starch-coated MNPs. The cortical neurons did not exhibit any significant change in viability even after incubation with the MNPs for up to 24 h (Appendix A Fig. A.1). Fluorescence intensity maps indicated that only cortical neurons stimulated with magnetic forces exhibited significant change in intracellular Ca^{2+} concentration (Fig. 2.3a). The $\Delta F/F_0$ (change in fluorescence over background fluorescence) for 30 selected neurons in different test conditions over 3 trials (*color*-coded) are plotted in Fig. 2.3b. In the presence of nano-magnetic forces, all the fluorescent intensity line traces were above background, with an average $\Delta F/F_0$ of 0.20. On the other hand, cortical neurons in all the other conditions without nano-magnetic forces did not exhibit significant deviation in their intracellular Ca^{2+} levels from the resting zero level. On closer examination, some fluorescent intensity line traces were below the resting zero level in the unstimulated conditions. This was due to the strong background fluorescence of the photoresist used for nano-magnetic chip fabrication and the limitation of bleach correction algorithm. Overall, 68% of the cortical neurons stimulated with nano-magnetic forces exhibited a $\Delta F/F_0 > 15\%$ while only ~3% of cortical neurons incubated with MNPs but without nano-magnetic force stimulation exhibited similar response (Appendix A Fig. A.2).

To understand whether Ca^{2+} spiking was affected by the nano-magnetic forces, 40 neurons over 3 trials were selected from each test condition and their record of Ca^{2+} spikes over 5 min were tabulated with raster plots (Fig. 2.3c). Each cortical neuron was given an identity (ID) number and their fluorescent intensities were traced over 5 min. We observed that nano-magnetic forces increased the frequency of Ca^{2+} spiking in cortical neurons much more significantly than all the other cases

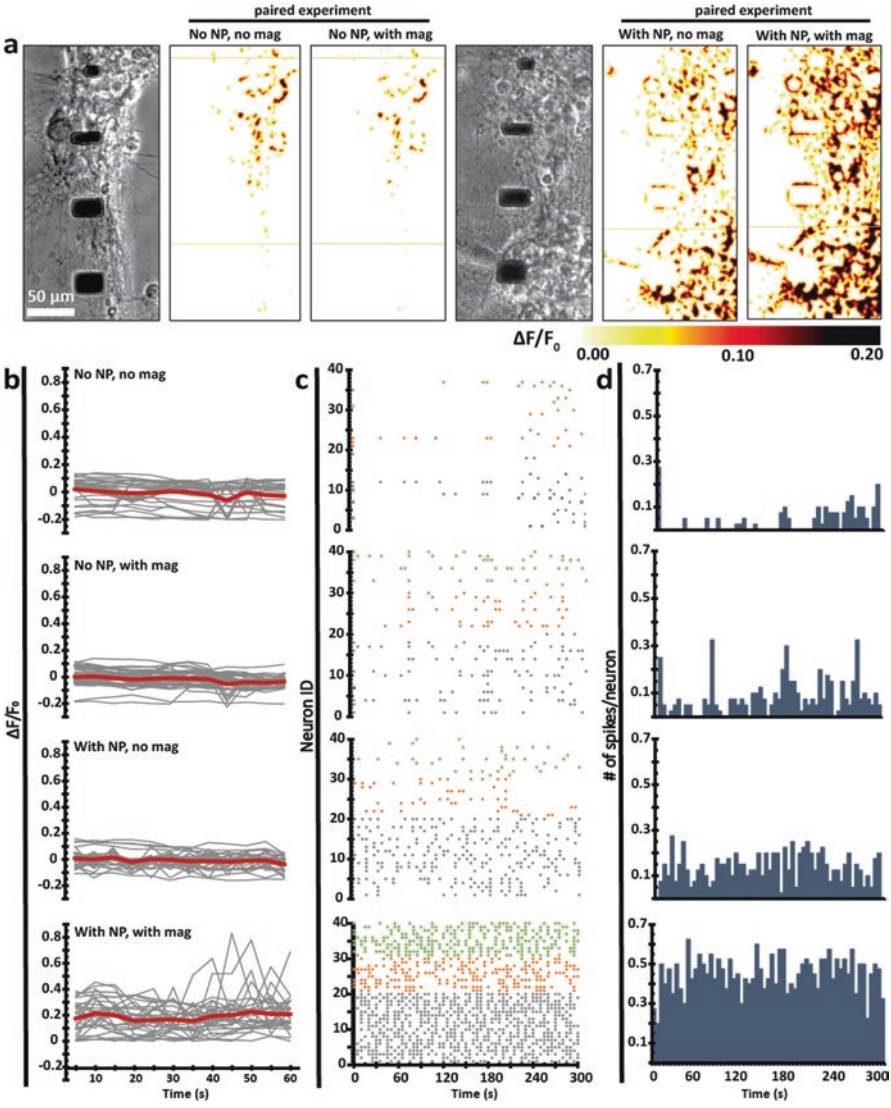

Fig. 2.3 Neurons that experienced nano-magnetic forces showed a larger change in calcium fluorescence intensity and spiking frequencies. (**a**) Color maps of fluorescence intensity change for different conditions. (**b**) Example fluorescence calcium concentrations ($\Delta F/F_0$) of 30 neurons for different conditions. (**c**) Raster plot of 40 neurons from three independent trials (first trial: grey, second trial: orange, third trial: green). An increase in spiking frequencies was observed for neurons stimulated with nano-magnetic forces. (**d**) Peristimulus time histograms of the raster plots binned at 5 s. All experiments with and without MNPs were paired

without nano-magnetic force stimulation. The number of spikes per cortical neuron at different time points (binned at 5 s) was also much higher in the stimulated cortical neural network (Fig. 2.3d).

2.2.5 *The Location of MNPs Affected the Response of Cortical Neural Networks to Nano-Magnetic Forces*

To determine whether the properties of MNPs could affect the response of the cortical neurons to nano-magnetic force stimulation, we also stimulated cortical neural network with chitosan-coated MNPs that tended to be internalized. Although a statistically significant change in $\Delta F/F_0$ was observed with both chitosan- and starch-coated MNPs (Student's t-test, $p < 0.05$) (Fig. 2.4a, b), $\Delta F/F_0$ in both cases differed by close to 9%. This difference could be due to the preferential localization of starch-coated MNPs at the cell membranes while the chitosan-coated MNPs tended to be internalized within intracellular compartments. More extensive interactions of starch-coated MNPs with membrane ion channels may result in larger Ca^{2+} influx [22]. It is also useful to note that in serum-free media like what we have used, nanoparticles were more likely to attach to the cell membrane, potentially allowing the MNPs to interact to a larger extent with membrane ion channels [27].

2.2.6 *Mechanism of Stimulation*

We first investigated the source of Ca^{2+} influx and found that when extracellular Ca^{2+} was depleted with EGTA or when there was no extracellular Ca^{2+}, the fluorescence signal was quenched whereas when intracellular Ca^{2+} was depleted with

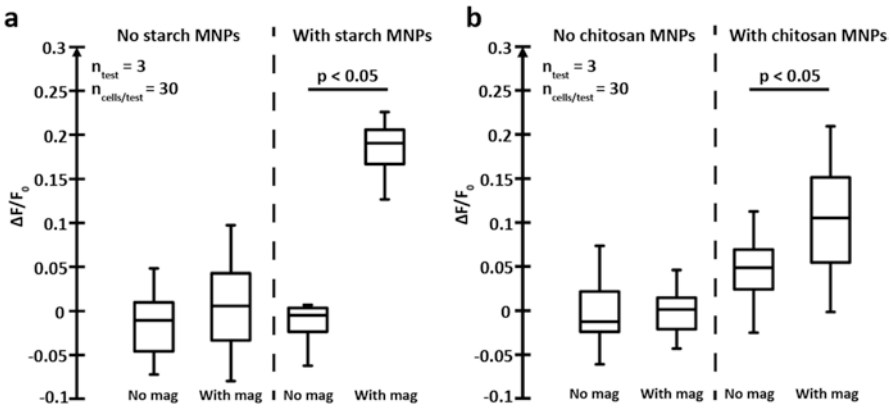

Fig. 2.4 Nano-magnetic force stimulation varies with functional groups on MNPs. (**a**) $\Delta F/F_0$ (n = 360) indicated significant changes in calcium fluorescence intensity due to nano-magnetic forces from starch-coated MNPs. (**b**) $\Delta F/F_0$ due to magnetic forces from chitosan-coated MNPs was statistically compared to condition without nano-magnetic forces but had less effects than that for starch-coated MNPs. We hypothesize that the difference in the degree of activation might be due to the preferential localization of starch-coated MNPs at the membrane of the neurites. This might have increased interactions of MNPs with mechano-sensitive ion channels, giving rise to larger calcium influx. On the other hand, chitosan-coated MNPs tended to be internalized by the neural network and hence experienced less interactions with ion channels

thapsigargin there was only a delay in the increase in fluorescence intensities (Fig. 2.5a). This suggests that magnetically induced Ca^{2+} influx was not G-protein mediated which typically involves release of Ca^{2+} from intracellular sources [32]. To further confirm, we also performed magnetic stimulation in the presence of 3 μM of bicuculline (EC_{50}), an inhibitor of γ-aminobutyric ($GABA_A$) receptor which is expressed widely in the brain, and observed higher Ca^{2+} spiking frequencies in the neurons upon magnetic stimulation (Fig. 2.5b). These two experiments show that magnetically induced Ca^{2+} influx was not modulated by G-protein and $GABA_A$ antagonist. We rationalized that if magnetic forces could increase $\Delta F/F_0$ in the presence of bicuculline, it would also mean that magnetic stimulation did not inactivate inhibitory ion channels/receptors.

The next logical step was to determine if magnetic forces activated excitatory ion channels. We found that the amplitude of the magnetic forces (Appendix A Fig. A.3) shared a skewed sigmoidal relationship to the Ca^{2+} fluorescence signals (Fig. 2.5c). The amplitude of Ca^{2+} fluorescence signals is a product of the conductance (g), number density (N), and open probability (P_{open}) of the ion channel. In order to change the conductance of the ion channel, the permeation pore which is a highly conserved structure must be modified and structural changes usually result in blocking than enhanced permeability [33]. We also did not expect and observe any changes in the number density from acute stimulation as the timescale during stimulation (~5–10 min) is much less than the time (~h) needed for ion channel transcription/translation. Hence we reasoned that the applied forces enhanced the open probability of the ion channel, thereby facilitating Ca^{2+} influx which is supported by a previous study [34].

The sigmoidal relationship between force amplitude and calcium fluorescence signals has been previously observed in mechano-sensitive ion channels [34], suggesting to us that magnetic forces might have activated mechano-sensitive Ca^{2+} channels especially concentrated at the boutons (Fig. 2.5dii). This hypothesis was also motivated by our observation that starch-coated MNPs preferentially localized to the membrane rather than being internalized where the membrane-bound MNPs could have stretched the lipid membrane to open mechano-sensitive ion channels.

To show that our method of stimulation was not voltage dependent, we first added 1 μM tetrodotoxin (TTX), a highly specific inhibitor of voltage-gated sodium channels involved in action potential propagation. We observed apparent stimulatory effects due to magnetic forces even with TTX (Fig. 2.5e). We also administered 40 mM potassium ions (K^+) to induce action potentials and found that when magnetic forces were applied there was still albeit a small increase in Ca^{2+} fluorescence intensity (Fig. 2.5f). Collectively, these two pieces of data suggest that our method of stimulation is not voltage dependent.

As neurons express many types of mechano-sensitive ion channels (Appendix A Table A.3), we thus attempted to identify the type of known channel that contributed most to the Ca^{2+} influx. We first inhibited the N-type mechano-sensitive calcium ion channels with a highly specific inhibitor, i.e., ω-conotoxin GVIA (1 μM), and found that this completely quenched the stimulatory effects of magnetic forces (Fig. 2.5g). As L-type Ca^{2+} channel is reportedly mechano-sensitive but it undergoes rapidly

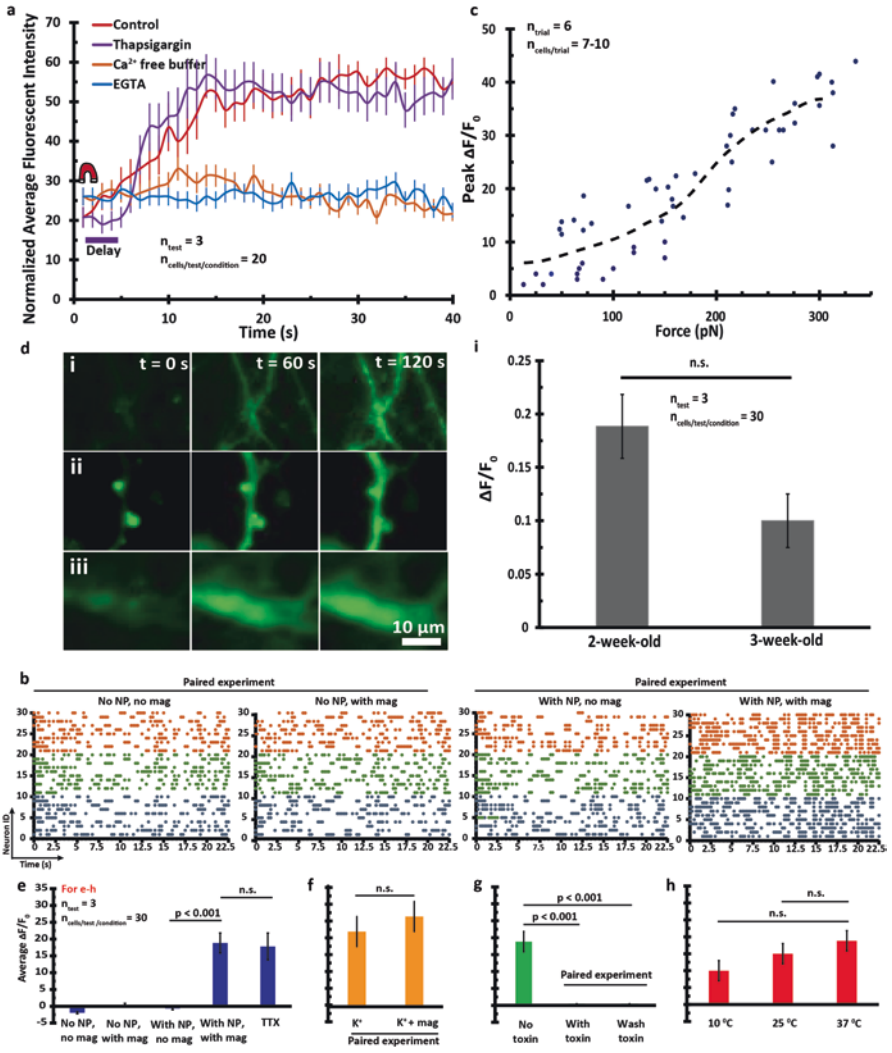

Fig. 2.5 Mechanism for magnetic stimulation of neural networks. (**a**) Magnetic stimulation leads to influx of calcium primarily from the extracellular environment. (**b**) Magnetic forces increased calcium spiking in the presence of bicuculline, suggesting that this technique is not neurotransmitter mediated and does not inactivate inhibitory ion channels for calcium influx. (**c**) The amplitude of the magnetic force shared a sigmoidal relationship to the peak $\Delta F/F_0$, suggesting the possibility of controlling stimulation dosage by changing the probability of ion channel opening. (**d**) Time-lapsed images show increase in calcium fluorescence signals in (**i**) dendrites, (**ii**) axonal boutons where presynaptic terminals are located, and (**iii**) cell body. Magnetic stimulation induced ~20% increase in average $\Delta F/F_0$ even in the presence of (**e**) TTX and (**f**) K^+, showing that voltage-gated ion channels were not activated. (**g**) Inhibition with ω-conotoxin GVIA quenched calcium influx even after washing, supporting that mechano-sensitive N-type calcium channels were involved. (**h**) Magnetic stimulations were not temperature sensitive, hence ruling out the possibility of activating TRP ion channels which are heat/mechano-sensitive. (**i**) Three-week-old neurons experience less calcium influx with magnetic stimulation

reversible inhibition by ω-conotoxin GVIA [35], we also performed a wash step, followed by subsequent monitoring of Ca^{2+} fluorescence signals. We did not observe any restoration of stimulatory effects of magnetic fields 10 min after washing away the neurotoxin (Fig. 2.5g), suggesting that neural stimulation did not involve L-type Ca^{2+} channels.

We next performed magnetic stimulation at different temperatures and found that the $\Delta F/F_0$ was not heat sensitive (Fig. 2.5h), hence ruling out that we are activating temperature-sensitive TRP ion channel which is also a major class of mechano-sensitive ion channel. This finding is also aligned with the knowledge that static magnetic field does not generate heat. The lower calcium influx at lower temperatures could be due to lower metabolism for uptake and intracellular trafficking of calcium indicators. Based on the literature review summarized in Appendix A Table A.3, there are also a few other reasons why we believe we did not perturb TRP ion channels with magnetic stimulation: (1) TRP ion channels are mostly located on neurons in the dorsal root ganglion (DRG) where they play a role in touch/pain sensation while we cultured cortical neurons; (2) Chen et al. have shown that without genetically transfecting neurons to significantly increase their expression of TRPV ion channels, there was no Ca^{2+} influx even with thermal stimulation; [15] (3) TRP ion channels possess intracellular Ankyrin domains that allow mechano-sensing by tethered channels and not the lipid bilayer model that we proposed [36]. One other class of mechano-sensitive ion channel that the magnetic forces might have perturbed is PIEZO2 [37] which is a newly discovered ion channel without any specific inhibitor yet [38]. However, we reasoned that as they are mostly located on DRG neurons and have much lower expression in the cortices as compared to mechano-sensitive N-type calcium channels, their contribution to Ca^{2+} influx would be insignificant even if they were activated.

Lastly, we wanted to understand whether the age of neurons, which we have found to affect their interactions with MNPs [39], could impact neural response to magnetic stimulation. We found that $\Delta F/F_0$ was lower for older neurons (Fig. 2.5i), possibly due to differences in ion channel expression such as reduction in expression of mechano-sensitive N-type Ca^{2+} channel with age [40].

Together, our results support a mechanism whereby magnetic stimulation induced calcium influx through activating N-type excitatory Ca^{2+} channels which are mechano-sensitive. Our hypothesis is that the preferential location of starch-coated MNPs at the cell membrane could have led to membrane stretching and activation of these channels that are concentrated at the presynaptic terminals.

We, however, do not rule out the possibility that other mechano-sensitive ion channels might have contributed to the Ca^{2+} influx as there could be unknown ion channels or undiscovered properties of known ion channels. Furthermore, mechano-sensing either by conformational changes in the lipid membrane or by tethered channels might not be mutually exclusive [36] as magnetic forces might also indirectly induce cytoskeletal movements. Our argument is hence similar to thermo/magneto-genetics where it is expected that the applied heat or mechanical stimuli might also activate intrinsic heat/mechano-sensitive ion channels [41–44]. Although there is a possibility that other mechano-sensitive ion channels might be

activated by magnetic force-induced stretching of lipid membrane, we showed that the contribution by N-type Ca^{2+} channels was the largest (Fig. 2.5g). We understand that there is a possibility that the applied magnetic forces could activate excitatory mechano-sensitive TRPV4, PIEZO1, and NMDA receptors. Future work is needed to apply a consistent method to quantify the force sensitivity of these different channels/receptors to compare or construct a model. It has been shown that a force of 3 pN could enhance the opening probability of mechano-sensitive ion channels in the hair cells of ears through mechanical amplification [45], suggesting that larger forces of 200–350 pN without amplification could be sufficient to generate the same effects on N-type Ca^{2+} channels present on each neuron. Recently, Wu et al. also found that a force of ~10 pN is needed to activate a single PIEZO ion channel. Consequently, the total force of 200 pN is only able to activate ~20 PIEZO ion channels which will be insufficient to generate the large calcium influx ($\Delta F/F_0 = 20\%$) that we observed. Therefore, based on the expression density, location, and responsive stimuli of the ion channels, we reasoned that it was most likely that magnetically induced Ca^{2+} influx was largely through the N-type Ca^{2+} channels.

2.2.7 Lipid Bilayer Stretch Model

There are currently two main models proposed for the gating process of mechano-sensitive ion channels, i.e., lipid bilayer stretch model and springlike tether model [46]. In the lipid bilayer stretch model, mechanical stimulations of the lipid bilayer trigger conformational changes to the mechano-sensitive ion channels, causing channels to open. In the springlike tether model, a springlike tether is associated with the mechano-sensitive ion channels, and upon tether deflection, the channels will open. From Fig. 2.2, we observed that starch-coated MNPs preferentially localized at membranes but we did not observe their preferential localization along the axons where N-type calcium ion channels are mostly located [47]. Therefore, we ruled out the springlike tether model where specific binding of starch-coated MNPs to proteins along the axons is needed for mechano-activation. A proposed model based on lipid bilayer stretching is shown in Fig. 2.6 where nano-magnetic force stimulates the opening of mechano-sensitive N-type Ca^{2+} ion channels for Ca^{2+} influx.

2.3 Conclusions

Biomedical applications of magnetic forces are becoming increasingly common. Magnetic forces have been reportedly used to improve transfection rates [48], gene therapy [49], stem cell differentiation [50], and tissue engineering [51]. For instance, Kriha et al. have previously described the production of electrospun fibers containing MNPs whose movements can be controlled to establish connections between

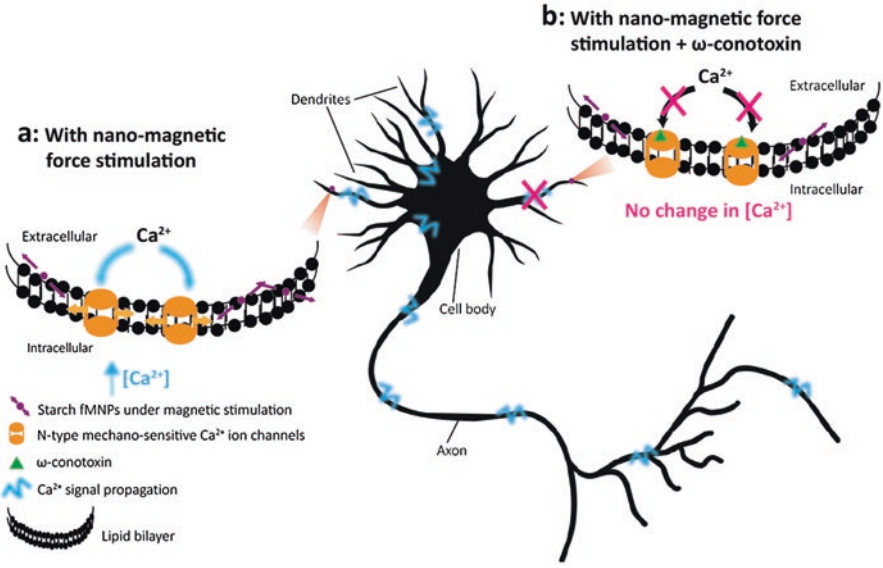

Fig. 2.6 Graphical illustration of proposed mechanism of nano-magnetic force stimulation. (**a**) In the presence of nano-magnetic forces, starch-coated MNPs localized at membranes could exert mechanical forces on the membranes, resulting in calcium influx through N-type mechano-sensitive calcium ion channels. The calcium signals are then propagated through the neurons and throughout the cortical neural networks. (**b**) In the presence of ω-conotoxin GVIA, calcium influx is inhibited even with nano-magnetic force stimulation as N-type mechano-sensitive calcium ion channels are blocked

hippocampal neurons to facilitate neural repair [52]. Similarly, Sakar and colleagues also utilized magnetic forces to manipulate the positions of neurons with micro precision and to deliver microgels to patterned neurons [53]. Xie et al. have also covalently linked nerve growth factor to magnetic nanotubes to induce differentiation in PC-12 cells [54].

There are also a few other pieces of literature that directly described the effects of magnetic forces on neuronal growth and neurite development. Fischer et al. made use of MNPs conjugated with anti-β-1 integrin to bind to neurons, followed by the application of magnetic forces to the neuron with a high-gradient electromagnet [55]. Using this technology, the group better understood the force dependence of neurite initiation. They demonstrated the formation of synapses between axons and dendrites in about half the experiments with magnetic forces and found that as the neurons mature it became increasingly less probable for magnetic forces to initiate neurite formation. Kim and colleagues also reported the use of static magnetic fields to elicit neurite outgrowth in PC-12 cells and the orientation of neurite growth was perpendicular to the direction of the applied magnetic field [24]. The team found that magnetic field could polarize the localization of actin and microtubules but did not change the levels of synaptotagmin responsible for synaptic formations. Nonetheless, in these papers, the authors recognize that they did not demonstrate a

connection between signaling cascades and the reported morphological change in neurite outgrowth, which we attempt to answer in our piece of research.

From the work of Mannix and coworkers, the group demonstrated that nano-magnetic forces could be transduced into physiological cellular outputs [56]. Briefly, the team conjugated MNPs with monovalent ligands, allowing the MNPs to bind to membrane receptors on cancer cells. Nano-magnetic forces were then applied to aggregate the membrane receptors, resulting in elevated intracellular Ca^{2+} concentrations within 20 s after the magnetic field was applied. Nonetheless, this work could not be directly translatable to neurons which have different Ca^{2+}-mediated signaling cascades as compared to cancer cells. Furthermore, the role of specific ion channels that elicit Ca^{2+} influxes was not investigated.

Utilizing tools from microfabrication and Ca^{2+} imaging, we demonstrate, to the best of our knowledge, the first time that nano-magnetic forces are able to induce Ca^{2+} influxes in cortical neural networks. We observed that the choice of coating on MNPs can affect their localization on the cortical neural network and subsequent strength of induction. Particularly, we saw that starch-coated fMNP had lower internalization than its chitosan-coated counterpart possibly due to its more negative zeta potential which is known to limit the uptake [28]. Interestingly, the inhibition of endocytosis with sodium azide did not affect the uptake of starch-coated MNPs significantly, suggesting the possibility of this type of nanoparticle localizing on the cell membranes instead of being internalized, supported by our fluorescence imaging results.

We then compared the $\Delta F/F_0$ in Ca^{2+} signals of the cortical neural network between starch-coated and chitosan-coated MNPs and found that the former was able to elicit a larger response. We hypothesized that this could be due to more extensive interactions of the membrane-bound starch-coated MNPs with membrane ion channels. To test our hypothesis, we inhibited the N-type Ca^{2+} ion channels with ω-conotoxin GVIA and found that even after washing away the toxin the inhibitory effects were not rapidly reversible. These results supported our hypothesis that the applied nano-magnetic forces could be stimulating mechano-sensitive N-type Ca^{2+} ion channels [57] although other ion channels could be involved as well [8]. Nonetheless, based on the amplitude and the duration (in the minute scale) of the transients after nano-magnetic force stimulation, Ca^{2+} was most likely the main ion involved [58].

In our work, we also demonstrated the remote activation of Ca^{2+} ion channels with high spatial resolution. Cortical neurons about 200 μm away from the magnetic elements did not experience significant change in intracellular levels. In human patients, the ability to spatially control the effects of magnetic field on Ca^{2+} influx may be achieved with precise implantations of magnetic chips similar to common procedures for deep brain stimulation using electrodes [59]. The recent invention of an electromagnetic microneedle actuator, which even when placed externally is capable of providing a high-gradient magnetic field with deep penetration [60], may remove the need for invasive implantations. Therefore, magnetic fields which are less attenuated by the body tissues compared to electric fields can provide greater efficacy in stimulating dysfunctional brain circuits.

The nano-magnetic force stimulation also elicited the propagation of Ca^{2+} influxes throughout the cortical neural network that was not demonstrated by recent work such as by Marino et al. who showed only a rise in intracellular Ca^{2+} levels in individual neurons [8]. The ability to demonstrate propagation of Ca^{2+} signals is significant as the neuroscience community increasingly advocates using neural networks instead of individual neurons as the paradigm for studying neuro-activities [16].

Through extensive experiments, we also demonstrated that magnetic forces most possibly induced Ca^{2+} influx by mechanically stretching the lipid membrane to modulate the open probability of mechano-sensitive N-type Ca^{2+} channels. One of our future planned experiments is to perform single-ion-channel patch clamping with a customized non-magnetic recording apparatus to eliminate electrical noise from the magnetic field to better understand the effects of magnetic forces on channel conductance and probability of channel opening. One way to increase the specificity of acute stimulation with this technique is to coat the MNPs with antibodies targeting the N-type calcium ion channel as proposed by Souza et al. [61] although this might be incompatible with chronic stimulation as the functions of the ion channels might be adversely affected.

There are a few ways to boost the magnitude of Ca^{2+} influx to match findings reported in the literature for orthogonal techniques [15]. Firstly, as nanoparticle uptake is stochastic in nature [62], functionalized MNPs [63] can be used to target specific mechano-sensitive ion channels on neurons. For instance, MNPs with more negative zeta potential may localize better at negatively charged cell membranes [28]. Targeted MNPs may also provide a causal evaluation of the role of specific cells (excitatory vs. inhibitory neurons) in the neural network. The same objective can also be achieved by increasing expression of N-type Ca^{2+} channels in the neurons similar to current practices in opto/thermogenetics or transfecting cells with constructs of genes encoding for magnetosomes from magnetotactic bacteria [64]. Next, steeper magnetic gradients or stronger magnets may find utility in inducing larger Ca^{2+} influx based on the observation that regions of neural network experiencing greater nano-magnetic forces also experienced greater $\Delta F/F_0$. Lastly, the use of ultrasensitive fluorophores such as GCaMPs [65] may also provide a better understanding on the timescale of the magnetic force-induced Ca^{2+} influx that were not captured by less sensitive fluo-4- and rhod-3-based fluorophores that we have used.

2.4 Materials and Methods

2.4.1 Fabrication of Magnetic Chips

Patterning of neurite networks was achieved on line-shaped PLL/Pluronic cell adhesive/repellent surface coatings. PLL lines were designed to be 100, 50, and 20 μm in width, adjacent to magnetic elements, which are embedded (1 μm deep) into a biocompatible photoresist and therefore shielded from the PLL surface. By monitoring the movements of microparticles, the magnetic field strength 1 μm

above the magnetic elements is ~0.73*B_{max} (applied magnetic field) [20]. Fabrication of the magnetic chips is based on previously described protocol [20]. Briefly, fused silica wafers (d: 10 mm, University Wafer) were cleaned in piranha solution (4:1) for 30 min, and oxygen plasma (air, 100 °C, 200 W, 2 min). A 50 nm Ti, 200 nm Cu, and 50 nm Ti seed layer was then evaporated onto the substrate. Microstructured SPR 220 photoresist formed 4 μm thick nickel-iron (NiFe, 80:20) alloys during electroplating. Residual titanium and copper layer was subsequently etched in 1% HF and copper etchant (5% acetic acid, 15% H_2O_2), respectively. The NiFe magnetic elements were passivated by 100 nm PECVD SiN and planarized by 5 μm of 1002F. A second lithography layer (SPR 220–3) was performed on top of the planarizing 1002F4 layer to produce striped openings for cell adhesion patterning. Chips were stored at room temperature shielded from light until further usage. Prior to each neuronal cell seeding, opened 1002F structures were O_2 plasma activated (38 W, 45 s, 500 mTorr) and SPR 220–3 was removed through a 100% acetone rinse. A polymeric 0.05% (w/v) Pluronics, 25% (v/v) PLL in PBS solution, was subsequently co-adsorbed to oxygen plasma-activated surface, after 20-min UV sterilization for 16 h at 37 °C. Prior to cell seeding, polymeric solution was aspirated, andchips were washed with sterile water and culture medium (Neurobasal).

2.4.2 Cortical Neural Culture

Whole-brain rats (E18, Brainbits) were transferred to PBS (33 mM glucose) and 1% (v/v) penicillin-streptomycin (PenStrep from Gibco®) and washed for 5 min and cortical hemispheres dissected [20]. Cortical tissues were then placed in Papain/Hibernate-E (pH 7.3, 10% (v/v) Carica papaya, Roche) and dissociated for 15 min at 37 °C. Ten percentage of horse serum (Fisher Sci) in Neurobasal (Gibco®) was then added to quench the enzymatic activity of Papain and the dissociated tissues were triturated through a 1000 μL pipette tip and filtered through a 40 μm cell strainer. Cell count was determined and one million cells were seeded onto each magnetic chip. After 2 h of incubation (95% air, 5% CO_2, 37 °C), unattached cells were washed away with pre-warmed culture media.

2.4.3 Characterization of Nanoparticle Properties

ZetaPALS 90Plus particle size analyzer was used to determine the hydrodynamic diameter of the nanoparticles. Briefly, nanoparticles were suspended (54,000 × 10^6 nanoparticles/mL) and pipetted into a cuvette before measurement with a laser via dynamic light scattering. A smooth auto-correction/error function was obtained before data collection, following which the ZetaPLAS zeta potential analyzer with electrode probe AQ599 was used to determine the zeta potential of the

nanoparticles. It is important to enter the right size of the nanoparticles to reduce fluctuations of the zeta potential readings.

2.4.4 Nanoparticle Incubation

Cortical neurons were incubated with starch- or chitosan-coated fMNPs (Chemicell) for 2, 6, or 24 h at 0.12% (v/v) in Neurobasal, 1% PenStrep, 1% GlutaMAX™, and 2% B27 supplement, after which the cells were gently washed three times with Neurobasal media to remove excess of fMNPs. The fMNPs are composed of magnetite with either starch or linear chitosan randomly distributed around the magnetite core. The density of the fMNPs is 1.25 g/cm^3. The size of the fMNPs according to the manufacturers is 100 nm. However, our measurement with dynamic light scattering shows that the hydraulic diameter of the fMNPs is in the range of ~200 nm (starch coated) and ~400 nm (chitosan coated). As fMNPs are also frequently used for localized heating, additional information on magnetic hysteresis can also be useful for readers. For interested readers: the TEM images and magnetic hysteresis curves of the iron oxide core can be obtained from Eggeman et al. [66]; the magnetic hysteresis curves of starch-coated and chitosan-coated fMNPs are also available from Cole et al. [67] and Kong et al. [68], respectively.

2.4.5 Calcium Dye Incubation and Magnetic Force Stimulation

Cortical neurons were incubated with Fluo-4 Direct™ calcium assay kit (Life Technologies) or Rhod-3 calcium imaging kit (Life Technologies) according to the manufacturer's protocol with 5 mM stock solution of probenecid. Briefly, 5 mL of calcium assay buffer was mixed and vortexed with 100 μL of probenecid stock solution to create a 2× loading dye solution. The dye solution is then added to the cells with media in a 1:1 ratio and incubated for 1 h before imaging. For magnetic force stimulation, calcium activity was monitored without a permanent magnetic field (OFF), and with a neodymium magnet (ON: B_{max} = 150 mT, ½ inch × ½ inch × ½ inch, Apex Magnets) placed on top of an inverted chip. For experiments involving TTX (1 μM), K^+ (40 mM), ω-conotoxin GVIA (1 μM), thapsigargin (2 μM), EGTA (10 mM), and bicuculline (3 or 1.2 μM), the chemical was added during calcium dye incubation (1 h). The use of EGTA is to completely chelate extracellular calcium. The method is to confirm that the source of calcium is from the extracellular environment as there is usually still some residual calcium from the neuronal media even after replacement with calcium-free buffer. After imaging, the solution was replaced with fresh media and the cortical neural network was imaged again. For experiments involving ω-conotoxin GVIA, a wash step was also included to remove the neurotoxin and the neurons were imaged after 15 min of waiting time.

2.4.6 Immunofluorescent Labeling

Cortical neurons were washed with Dulbecco's PBS with magnesium and calcium (Gibco) and fixed with paraformaldehyde (4% v/v, Santa Cruz Biotechnologies), permeabilized with 0.1% Triton-x/DPBS and 3% BSA for 10 min, and blocked with 3% goat serum in 1% BSA/DPBS. Primary antibodies were incubated overnight at 4 °C in 3% goat serum and 0.5% Tween-20 in 1% BSA/DPBS and secondary antibodies were added. Finally 4′,6- diamidino-2-phenylindole (DAPI, 300 nM in DPBS) was incubated for 15 min and additionally mounted on glass slides using pro ProLong® Gold antifade reagent (Molecular Probes).

2.4.7 Cytotoxicity Assay

Colorimetric MTT (3-(4,5-dimethylthiazol-2-yl)-2,5-diphenyltetrazolium bromide) assays were performed in 96-well plates where different functionalized fMNPs were added to each well seeded with cortical neurons. After each specific time interval, 20 μL of MTT (5 mg/mL) in PBS was incubated for 3 h. Then the supernatant was aspirated and 200 μL of dimethyl sulfoxide (DMSO) was added. Each 200 μL sample in DMSO was spun down to remove MNPs in solution and the supernatant was read with a 96-well plate reader for absorbance at 550 nm.

2.4.8 Flow Cytometry Analysis

1.0×10^6 neurons were seeded in individual PLL-coated 12-well plate (Corning) and allowed to grow for 2 weeks. Fluorescently labeled MNPs (green: ex (476 nm), em (490 nm); red: ex (578 nm), em (613 nm)) were then added at a concentration of $54{,}000 \times 10^6$/mL and incubated for 24 h before triple washing with neural basal media. For experiment involving sodium azide, cortical neurons were also incubated with 5 mg/mL sodium azide solution for 24 h. Neurons were then detached from plate surface using Accutase® (Stemcell Technologies, ref # A11105-01) for 10 min and centrifuge at 600 g for 6 min to collect the pellet. Cell pellet was then resuspended in 500 μL DPBS, stored at 4 °C, and analyzed using BD LSRII flow cytometer at the UCLA Flow Cytometry Core Laboratory.

2.4.9 Image Acquisition, Analysis, and Statistical Evaluations

Wide-field fluorescent and phase-contrast images were acquired with an inverted fluorescent microscope (Nikon, 20×, 40× air, 60× air objective) or confocal microscope (Leica TCS SP5, 60× oil objective). The fixed and immune-stained samples

were excited with 364 nm (blue/DAPI), 488 nm (green/MAP2), 650 nm (Cy5/TAU), and 532 nm (red/fluorescent fMNPs) laser lines.

Heat maps were generated with ImageJ plug-in HeatMap from Stack. Parameters (color min/max) were kept consistent for comparison of calcium fluorescence.

The relative fluorescence change $\Delta F/F_0$ of somatic fluorescence signals was acquired using ImageJ for all neurons within a particular trial. Calcium spike events were considered if they fulfilled two criteria: (1) the fluorescence increase was at least five standard deviations above baseline, which was defined as first 5 s of each trace and (2) if the event persisted more than 5 s. Raster plots were then generated from this method. Calcium videos were taken over 5 min with a per frame period of 5 s.

Transmission electron microscopy (TEM) images of the starch-coated fMNPs were acquired with a T12 Quick CryoEM with exposure time of 0.5 s. Briefly, the starch-coated fMNPs ($45{,}000 \times 10^6$/mL) were incubated with Neurobasal media for 6 h and then centrifuged at 600 g for 6 min to collect the pellet. The pellet was resuspended in 50 μL deionized water. The starch-coated fMNPs were then adsorbed onto 400-mesh copper grid coated with carbon (Ted Pella Inc.). TEM was performed using 120 kV T12 Quick CryoEM with a point resolution of 0.34 nm. Imaging and data processing were performed at the UCLA CNSI Electron Imaging Center for NanoMachines (EICN).

Statistical significance in Fig. 2.2b was evaluated using Mann–Whitney U Test with null hypothesis = 0 and $n = 30{,}000$ (3 tests, 10,000 cells/test). Statistical significance in Fig. 2.5 and Appendix A Fig. A.1 was evaluated using Student's t-test after testing for normality using either one-way ANOVA, $p < 0.05$ (no rejection of normality), or nonparametric Kruskal-Wallis ANOVA, $p < 0.05$ (normality rejected), with $n = 120$ cells in Fig. 2.5a (3 tests, 4 conditions, 10 cells/test/condition), $n = 120$ cells in Fig. 2.5b (4 condition, 30 cells/condition), $n = 42$–60 cells in Fig. 2.5c ($n_{\text{trials}} = 6$, 7–10 cells/test), $n = 60$ cells in Fig. 2.5e (2 paired experiments, 3 tests, 10 cells/experiment), $n = 30$ cells in Fig. 2.5f/g (1 paired experiment, 3 tests, 10 cells/experiment), $n = 60$ cells in Fig. 2.5h (1 control and 1 paired experiment, 3 tests, 10 cells/experiment), $n = 90$ in Fig. 2.5i (3 conditions, 3 tests, 10 cells/experiment), and $n = 120$ (2 conditions, 2 tests, 30 cells/test/condition), $n = 360$ cells (4 groups, 3 trials, and 30 cells/trial), and $n = 600$ cells (6 test, 100 cells/test) in Appendix A Fig. A.1.

References

1. West, A.E., Chen, W.G., Dalva, M.B., Dolmetsch, R.E., Kornhauser, J.M., Shaywitz, A.J., Takasu, M.A., Tao, X., Greenberg, M.E.: Calcium regulation of neuronal gene expression. Proc. Natl. Acad. Sci. U. S. A. **98**, 11024–11031 (2001)
2. Mattson, M.P., LaFerla, F.M., Chan, S.L., Leissring, M.A., Shepel, P.N., Geiger, J.D.: Calcium signaling in the ER: its role in neuronal plasticity and neurodegenerative disorders. Trends Neurosci. **23**, 222–229 (2000)
3. Berridge, M.J., Bootman, M.D., Lipp, P.: Calcium--a life and death signal. Nature. **395**, 645–648 (1998)

4. Tsai, H.-C., Zhang, F., Adamantidis, A., Stuber, G.D., Bonci, A., de Lecea, L., Deisseroth, K.: Phasic firing in dopaminergic neurons is sufficient for behavioral conditioning. Science. **324**, 1080–1084 (2009)
5. Bernstein, J.G., Garrity, P.A., Boyden, E.S.: Optogenetics and thermogenetics: technologies for controlling the activity of targeted cells within intact neural circuits. Curr. Opin. Neurobiol. **22**, 61–71 (2012)
6. Banghart, M., Borges, K., Isacoff, E., Trauner, D., Kramer, R.H.: Light-activated ion channels for remote control of neuronal firing. Nat. Neurosci. **7**, 1381–1386 (2004)
7. Tyler, W.J., Tufail, Y., Finsterwald, M., Tauchmann, M.L., Olson, E.J., Majestic, C.: Remote excitation of neuronal circuits using low-intensity, low-frequency ultrasound. PLoS One. **3**, e3511 (2008)
8. Marino, A., Arai, S., Hou, Y., Sinibaldi, E., Pellegrino, M., Chang, Y.-T., Mazzolai, B., Mattoli, V., Suzuki, M., Ciofani, G.: Piezoelectric nanoparticle-assisted wireless neuronal stimulation. ACS Nano. **9**(7), 7678–7689 (2015)
9. Zemelman, B.V., Lee, G.A., Ng, M., Miesenböck, G.: Selective photostimulation of genetically chARGed neurons. Neuron. **33**, 15–22 (2002)
10. Boyden, E.S., Zhang, F., Bamberg, E., Nagel, G., Deisseroth, K.: Millisecond-timescale, genetically targeted optical control of neural activity. Nat. Neurosci. **8**, 1263–1268 (2005)
11. Sparta, D.R., Stamatakis, A.M., Phillips, J.L., Hovelsø, N., van Zessen, R., Stuber, G.D.: Construction of implantable optical fibers for long-term optogenetic manipulation of neural circuits. Nat. Protoc. **7**, 12–23 (2012)
12. Wang, N., Butler, J.P., Ingber, D.E.: Mechanotransduction across the cell surface and through the cytoskeleton. Science. **260**, 1124–1127 (1993)
13. Hughes, S., McBain, S., Dobson, J., El Haj, A.J.: Selective activation of mechanosensitive ion channels using magnetic particles. J. R. Soc. Interface. **5**, 855–863 (2008)
14. Huang, H., Delikanli, S., Zeng, H., Ferkey, D.M., Pralle, A.: Remote control of ion channels and neurons through magnetic-field heating of nanoparticles. Nat. Nanotechnol. **5**, 602–606 (2010)
15. Chen, R., Romero, G., Christiansen, M.G., Mohr, A., Anikeeva, P.: Wireless magnetothermal deep brain stimulation. Science. **347**, 1477–1480 (2015)
16. Yuste, R.: From the neuron doctrine to neural networks. Nat. Rev. Neurosci. **16**, 487–497 (2015)
17. Kisaalita, W.S., Evans, M., Lund, R.B.: Size changes in differentiating neuroblastoma cells. Vitr. Cell. Dev. Biol. - Anim. **33**, 734–737 (1997)
18. Clement, G.T., Nomura, H., Adachi, H., Kamakura, T.: The feasibility of non-contact ultrasound for medical imaging. Phys. Med. Biol. **58**, 6263–6278 (2013)
19. Steketee, M.B., Moysidis, S.N., Jin, X.-L., Weinstein, J.E., Pita-Thomas, W., Raju, H.B., Iqbal, S., Goldberg, J.L.: Nanoparticle-mediated signaling endosome localization regulates growth cone motility and neurite growth. Proc. Natl. Acad. Sci. **108**, 19042–19047 (2011)
20. Kunze, A., Tseng, P., Godzich, C., Murray, C., Caputo, A., Schweizer, F.E., Di Carlo, D.: Engineering cortical neuron polarity with nanomagnets on a chip. ACS Nano. **9**(4), 3664–3676 (2015)
21. Tay, A.K., Dhar, M., Pushkarsky, I., Di Carlo, D.: Research highlights: manipulating cells inside and out. Lab Chip. **15**, 2533–2537 (2015)
22. Dobson, J.: Remote control of cellular behaviour with magnetic nanoparticles. Nat. Nanotechnol. **3**, 139–143 (2008)
23. Jung, S., Bang, M., Kim, B.S., Lee, S., Kotov, N.A., Kim, B., Jeon, D.: Intracellular gold nanoparticles increase neuronal excitability and aggravate seizure activity in the mouse brain. PLoS One. **9**, e91360 (2014)
24. Kim, S., Im, W.S., Kang, L., Lee, S.T., Chu, K., Kim, B.I.: The application of magnets directs the orientation of neurite outgrowth in cultured human neuronal cells. J. Neurosci. Methods. **174**, 91–96 (2008)
25. Etoc, F., Vicario, C., Lisse, D., Siaugue, J.-M., Piehler, J., Coppey, M., Dahan, M.: Magnetogenetic control of protein gradients inside living cells with high spatial and temporal resolution. Nano Lett. **15**(5), 3487–3494 (2015)

26. Walkey, C.D., Olsen, J.B., Song, F., Liu, R., Guo, H., Olsen, D.W.H., Cohen, Y., Emili, A., Chan, W.C.W.: Protein corona fingerprinting predicts the cellular interaction of gold and silver nanoparticles. ACS Nano. **8**, 2439–2455 (2014)
27. Lesniak, A., Fenaroli, F., Monopoli, M.P., Åberg, C., Dawson, K.A., Salvati, A.: Effects of the presence or absence of a protein corona on silica nanoparticle uptake and impact on cells. ACS Nano. **6**, 5845–5857 (2012)
28. He, C., Hu, Y., Yin, L., Tang, C., Yin, C.: Effects of particle size and surface charge on cellular uptake and biodistribution of polymeric nanoparticles. Biomaterials. **31**, 3657–3666 (2010)
29. Gao, H., Yang, Z., Zhang, S., Cao, S., Shen, S., Pang, Z., Jiang, X.: Ligand modified nanoparticles increases cell uptake, alters endocytosis and elevates glioma distribution and internalization. Sci. Rep. **3**, 2534 (2013)
30. Westenbroek, R.E., Hell, J.W., Warner, C., Dubel, S.J., Snutch, T.P., Catterall, W.A.: Biochemical properties and subcellular distribution of an N-type calcium channel alpha 1 subunit. Neuron. **9**, 1099–1115 (1992)
31. Rao, W., Wang, H., Han, J., Zhao, S., Dumbleton, J., Agarwal, P., Zhang, W., Zhao, G., Yu, J., Zynger, D.L., et al.: Chitosan-decorated doxorubicin-encapsulated nanoparticle targets and eliminates tumor reinitiating cancer stem-like cells. ACS Nano. **9**, 5725–5740 (2015)
32. Patel, J.C., Witkovsky, P., Avshalumov, M.V., Rice, M.E.: Mobilization of calcium from intracellular stores facilitates somatodendritic dopamine release. J. Neurosci. **29**, 6568–6579 (2009)
33. Dworakowska, B., Dołowy, K., Tyson, J.R., Snutch, T.P., Piontkivska, H., Hughes, A.L., Bidaud, I., Mezghrani, A., Swayne, L.A., Monteil, A., et al.: Molecular nature of voltage-gated calcium channels: structure and species comparison. Wiley Interdiscip. Rev. Membr. Transp. Signal. **2**, 181–206 (2013)
34. Calabrese, B., Tabarean, I.V., Juranka, P., Morris, C.E.: Mechanosensitivity of N-type calcium channel currents. Biophys. J. **83**, 2560–2574 (2002)
35. McCleskey, E.W., Fox, A.P., Feldman, D.H., Cruz, L.J., Olivera, B.M., Tsien, R.W., Yoshikami, D.: Omega-Conotoxin: direct and persistent blockade of specific types of calcium channels in neurons but not muscle. Proc. Natl. Acad. Sci. U. S. A. **84**, 4327–4331 (1987)
36. Sabass, B., Stone, H.A.: Mechanosensing by tethered membrane channels. Bull. Am. Phys. Soc. **61**, 2 (2016)
37. Coste, B., Mathur, J., Schmidt, M., Earley, T.J., Ranade, S., Petrus, M.J., Dubin, A.E., Patapoutian, A.: Piezo1 and Piezo2 are essential components of distinct mechanically activated cation channels. Science. **330**, 55–60 (2010)
38. Zhao, Q., Wu, K., Geng, J., Chi, S., Wang, Y., Zhi, P., Zhang, M., Xiao, B.: Ion permeation and mechanotransduction mechanisms of mechanosensitive piezo channels. Neuron. **89**, 1248–1263 (2016)
39. Tay, A., Kunze, A., Jun, D., Hoek, E., Di Carlo, D.: The age of cortical neural networks affects their interactions with magnetic nanoparticles. Small. **12**(26), 3559–3567 (2016)
40. Chameau, P., Lucas, P., Melliti, K., Bournaud, R., Shimahara, T.: Development of multiple calcium channel types in cultured mouse hippocampal neurons. Neuroscience. **90**, 383–388 (1999)
41. Stanley, S.A., Gagner, J.E., Damanpour, S., Yoshida, M., Dordick, J.S., Friedman, J.M.: Radiowave heating of iron oxide nanoparticles can regulate plasma glucose in mice. Science. **336**, 604–608 (2012)
42. Stanley, S.A., Sauer, J., Kane, R.S., Dordick, J.S., Friedman, J.M.: Remote regulation of glucose homeostasis in mice using genetically encoded nanoparticles. Nat. Med. **21**, 92–98 (2014)
43. Stanley, S.A., Kelly, L., Latcha, K.N., Schmidt, S.F., Yu, X., Nectow, A.R., Sauer, J., Dyke, J.P., Dordick, J.S., Friedman, J.M.: Bidirectional electromagnetic control of the hypothalamus regulates feeding and metabolism. Nature. **531**(7596), 647–650 (2016)
44. Wheeler, M.A., Smith, C.J., Ottolini, M., Barker, B.S., Purohit, A.M., Grippo, R.M., Gaykema, R.P., Spano, A.J., Beenhakker, M.P., Kucenas, S., et al.: Genetically targeted magnetic control of the nervous system. Nat. Neurosci. **19**(5), 756–761 (2016)

45. Hudspeth, A.J.: Making an effort to listen: mechanical amplification in the ear. Neuron. **59**, 530–545 (2008)
46. Delmas, P., Coste, B.: Mechano-gated ion channels in sensory systems. Cell. **155**, 278–284 (2013)
47. Pravettoni, E., Bacci, A., Coco, S., Forbicini, P., Matteoli, M., Verderio, C.: Different localizations and functions of L-type and N-type calcium channels during development of hippocampal neurons. Dev. Biol. **227**, 581–594 (2000)
48. Cai, D., Mataraza, J.M., Qin, Z.-H., Huang, Z., Huang, J., Chiles, T.C., Carnahan, D., Kempa, K., Ren, Z.: Highly efficient molecular delivery into mammalian cells using carbon nanotube spearing. Nat. Methods. **2**, 449–454 (2005)
49. Plank, C., Schillinger, U., Scherer, F., Bergemann, C., Rémy, J.S., Krötz, F., Anton, M., Lausier, J., Rosenecker, J.: The magnetofection method: using magnetic force to enhance gene delivery. Biol. Chem. **384**, 737–747 (2003)
50. Santos, L.J., Reis, R.L., Gomes, M.E.: Harnessing magnetic-mechano actuation in regenerative medicine and tissue engineering. Trends Biotechnol. **33**, 471–479 (2015)
51. Ito, A., Akiyama, H., Kawabe, Y., Kamihira, M.: Magnetic force-based cell patterning using Arg-Gly-Asp (RGD) peptide-conjugated magnetite cationic liposomes. J. Biosci. Bioeng. **104**, 288–293 (2007)
52. Kriha, O., Becker, M., Lehmann, M., Kriha, D., Krieglstein, J., Yosef, M., Schlecht, S., Wehrspohn, R.B., Wendorff, J.H., Greiner, A.: Connection of hippocampal neurons by magnetically controlled movement of short electrospun polymer fibers – a route to magnetic micromanipulators. Adv. Mater. **19**, 2483–2485 (2007)
53. Sakar, M.S., Steager, E.B., Cowley, A., Kumar, V., Pappas, G.J.: Wireless manipulation of single cells using magnetic microtransporters. In: 2011 IEEE International Conference on Robotics and Automation, pp. 2668–2673. IEEE, Shanghai (2011)
54. Xie, J., Chen, L., Varadan, V.K., Yancey, J., Srivatsan, M.: The effects of functional magnetic nanotubes with incorporated nerve growth factor in neuronal differentiation of PC12 cells. Nanotechnology. **19**, 105101 (2008)
55. Fischer, T.M., Steinmetz, P.N., Odde, D.J.: Robust micromechanical neurite elicitation in synapse-competent neurons via magnetic bead force application. Ann. Biomed. Eng. **33**, 1229–1237 (2005)
56. Mannix, R.J., Kumar, S., Cassiola, F., Montoya-Zavala, M., Feinstein, E., Prentiss, M., Ingber, D.E.: Nanomagnetic actuation of receptor-mediated signal transduction. Nat. Nanotechnol. **3**, 36–40 (2008)
57. Tyler, W.J.: The mechanobiology of brain function. Nat. Rev. Neurosci. **13**, 867–878 (2012)
58. Rosenberg, S.S., Spitzer, N.C.: Calcium signaling in neuronal development. Cold Spring Harb. Perspect. Biol. **3**, 1–13 (2011)
59. Perlmutter, J.S., Mink, J.W.: Deep brain stimulation. Annu. Rev. Neurosci. **29**, 229–257 (2006)
60. Matthews, B.D., Lavan, D.A., Overby, D.R., Karavitis, J., Ingber, D.E.: Electromagnetic needles with submicron pole tip radii for nanomanipulation of biomolecules and living cells. Appl. Phys. Lett. **85**, 2968–2970 (2004)
61. Carvalho-de-Souza, J.L., Treger, J.S., Dang, B., Kent, S.B.H., Pepperberg, D.R., Bezanilla, F.: Photosensitivity of neurons enabled by cell-targeted gold nanoparticles. Neuron. **86**, 207–217 (2015)
62. Summers, H.D., Rees, P., Holton, M.D., Brown, M.R., Chappell, S.C., Smith, P.J., Errington, R.J.: Statistical analysis of nanoparticle dosing in a dynamic cellular system. Nat. Nanotechnol. **6**, 170–174 (2011)
63. Jiang, W., Kim, B.Y.S., Rutka, J.T., Chan, W.C.W.: Nanoparticle-mediated cellular response is size-dependent. Nat. Nanotechnol. **3**, 145–150 (2008)
64. Grünberg, K., Wawer, C., Tebo, B.M., Schüler, D.: A large gene cluster encoding several magnetosome proteins is conserved in different species of magnetotactic bacteria. Appl. Environ. Microbiol. **67**, 4573–4582 (2001)

65. Chen, T.-W., Wardill, T.J., Sun, Y., Pulver, S.R., Renninger, S.L., Baohan, A., Schreiter, E.R., Kerr, R.A., Orger, M.B., Jayaraman, V., et al.: Ultrasensitive fluorescent proteins for imaging neuronal activity. Nature. **499**, 295–300 (2013)
66. Eggeman, A.S., Majetich, S.A., Farrell, D., Pankhurst, Q.A.: Size and concentration effects on high frequency hysteresis of iron oxide nanoparticles. IEEE Trans. Magn. **43**, 2451–2453 (2007)
67. Cole, A.J., David, A.E., Wang, J., Galbán, C.J., Hill, H.L., Yang, V.C.: Polyethylene glycol modified, cross-linked starch-coated iron oxide nanoparticles for enhanced magnetic tumor targeting. Biomaterials. **32**, 2183–2193 (2011)
68. Kong, S.D., Zhang, W., Lee, J.H., Brammer, K., Lal, R., Karin, M., Jin, S.: Magnetically vectored nanocapsules for tumor penetration and remotely switchable on-demand drug release. Nano Lett. **10**, 5088–5092 (2010)

http://www.springer.com/978-3-319-69058-2

Acute and Chronic Neural Stimulation via
Mechano-Sensitive Ion Channels
Ping, A.T.K.
2018, XVII, 119 p. 33 illus., 32 illus. in color., Hardcover
ISBN: 978-3-319-69058-2